Sequential Modeling of Coal Volatile Combustion in Fluidized Bed Reactors

ARTICLE *in* ENERGY & FUELS · JULY 2012

Impact Factor: 2.79 · DOI: 10.1021/ef300710j

4 AUTHORS, INCLUDING:

Ali Eslami
Laval University
5 PUBLICATIONS **19** CITATIONS
SEE PROFILE

Abolhasan Hashemisohi
North Carolina Agricultural and Technical Stat…
4 PUBLICATIONS **19** CITATIONS
SEE PROFILE

Rahmat Sotudeh-Gharebagh
University of Tehran
133 PUBLICATIONS **902** CITATIONS
SEE PROFILE

energy&fuels

Article

pubs.acs.org/EF

Sequential Modeling of Coal Volatile Combustion in Fluidized Bed Reactors

Ali Eslami,[†] Abolhasan Hashemi Sohi,[†] Amir Sheikhi,[†,‡] and Rahmat Sotudeh-Gharebagh*

Process Design and Simulation Research Centre, Oil and Gas Processing Centre of Excellence, School of Chemical Engineering, College of Engineering, University of Tehran, P.O. Box 11155-4563, Tehran, Iran

ABSTRACT: A sequential model to predict the combustion behavior of a coal's volatile matter during coal gasification, simulated by propane in a combustor is introduced and evaluated. For this, an industrial fluidized bed combustor is divided into several submultiphase reactors based on the physical behavior of interacting phases. This is achieved by considering the volatile gas as a completely mixed stream passing through the emulsion phase and as plug flow through the bubble phase. To simulate the events inside each subreactor, two models were used: a dynamic two-phase model for hydrodynamic characterization (called the hydrodynamic submodel) and a reaction kinetic submodel for obtaining the chemical evolution of subreactors. Also, an energy balance and temperature-dependent distribution of bubble sizes were embedded in the model. Considering the physical and chemical characteristics of the system, it has become possible to specify the proper number of simulation stages by introducing a new dimensionless number. The model was compared to several sets of experimental measurements in terms of the most important operating parameters derived from the literature, and an excellent consistency was achieved. The main motivation behind the current study was to provide a reliable, yet easy-to-achieve, modeling and simulation methodology by fundamental chemical engineering concepts to predict aspects of the behavior of volatile matter in processes producing energy from coal. This work opens up a new way of modeling coal's volatile matter combustion, especially for its optimization and scale up.

1. INTRODUCTION

The energy crisis in the recent decades challenged many industries to find alternative energy sources such as light-fuel from coal and coal gasification and combustion.[1] Among the various ways of energy production, integrated coal gasification combined cycle has been introduced as one of the most reliable methods, which is reported to have a high carbon capture rate and low pollutant emissions.[2] In such a process, fluidized bed coal gasifiers play an important role in energy conversion, while maintaining environmentally threatening species emission at its lowest possible amount.[3] Therefore, study on such multiphase reactors is of a high importance in energy industries.

Fluidized bed gasifiers, as the heart of a gasification process, are highly affected by the volatile matter behavior during combustion. Mainly, up to half of the coal specific energy comes from its volatile contents.[3,4] Coal volatiles combustion, set free during a gasification process, have a noticeable impact on char combustion reaction rate,[5,6] outlet gas composition, heat and mass transfer inside the bed as well as the freeboard,[3] and mixing patterns. Meanwhile, a lot of experimental studies were conducted to identify volatile matter reaction rate and location inside gasifiers, which led to the introduction of critical bed temperatures.[7−11] Such temperature should be exceeded to have the whole combustion taken place inside the bed.[3,12−14]

From the operational point of view, the presence of solid particles, as a medium for fluidized bed combustion, has a dual effect on the reactor efficiency. At low enough temperatures (~1073 K),[3] particles act as a heat sink and inhibit the combustion[15] of volatile matter. This is mainly due to bed quenching and radical heterogeneous termination, respectively.[9,10,16] Moreover, the combustion rate is dominated by the degree of oxygen and volatile mixing.[7] The situation becomes more complicated when more than almost 10% w/w solid particles[3] is char particles (e.g., in industrial fluidized bed gasifiers). At such a condition, oxygen is fully consumed inside the lower parts of the bed, and intermediate species (e.g., CO) are more probable to escape from having a complete reaction.

Although several experimental works[3,6,17,18] were reported in the literature studying coal volatile combustion mimicked by using propane, few attempts have been made to model fluidized bed volatile combustors (e.g., refs 19−21) due to their complexity and the high nonlinearity of governing physical and chemical coupled equations. Besides, commercial process simulators are only able to simulate ideal reactors. Thus, this paper aims at providing a new pathway in modeling nonideal multiphase coal volatile combustion processes using fundamental concepts of chemical engineering, which are well-established even inside industrial process simulators.

2. MULTIPHASE REACTOR MODEL

Figure 1 shows a schematic of a fluidized bed combustor (FBC). A typical FBC consists of two main regions, namely, the dense bed and the freeboard.[22] The dense bed of a FBC is considered as a two-phase gas−solid fluidized bed, which is operated under turbulent fluidization condition.[23] This is then divided into two subreactors. One subreactor is representing gas−solid emulsion phase, and the other contains bubble phase. The two subreactors cannot be isolated from each other in real fluidized bed reactors. Therefore, a FBC is acting like a highly nonlinear system including several interacting chemical substances in various physical states. The main working fluid

Received: April 27, 2012
Revised: July 12, 2012
Published: July 16, 2012

dx.doi.org/10.1021/ef300710j | Energy Fuels 2012, 26, 5199−5209

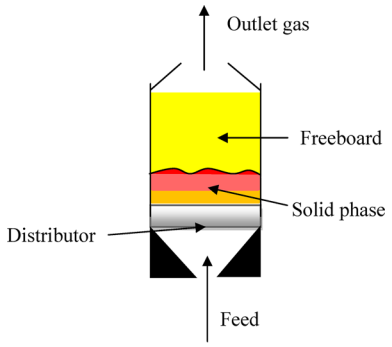

Figure 1. Schematic diagram of a fluidized bed combustor.

of a FBC is usually air or air/steam.[24] However, mixtures of air or air/steam and propane are also used for certain applications.[25] The bed material can be sand particles or a combination of sand and char. The fuel, which is coal, is fed into the reactor from the bottom. A heat source, such as a burner, is also used to heat bed materials to a given temperature and initiate reactions.

A FBC is a complex system; thus, it cannot be modeled using a single ideal reactor (e.g., whether a completely stirred tank reactor (CSTR) or a plug flow reactor (PFR)). A schematic of the so-called subreactors is presented in Figure 2. In this figure,

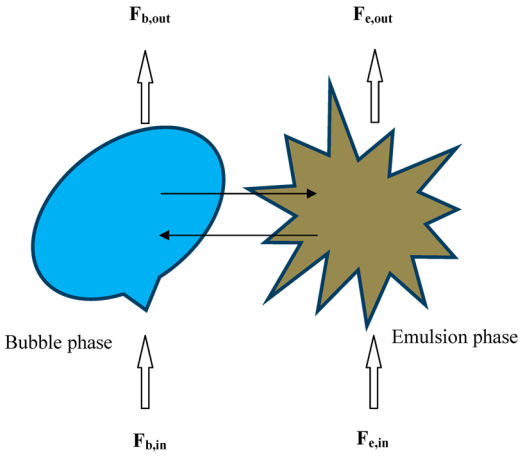

Figure 2. Interactions in the dense bed of a fluidized bed coal volatile combustion reactor.

the arrows show the overall interactions between two phases of emulsion and bubble, which are forming two subreactors. These interactions are mass and heat transfer. It is needed to interrelate the subreactors according to a logical manner. By considering the physical nature of each interacting phase, acting as one subreactor, it is found that the gas inside the bubbles is undergoing a plug flow because there is no mixing of solid and gas there. Moreover, the emulsion phase is experiencing a completely mixed medium.[26,27] Therefore, the gas inside the bubble phase can be considered as plug flow, and consequently, the subreactor can be treated as a PFR. Also, the passing gas through the emulsion can be considered as a fully mixed medium; thus, the corresponding subreactor is treated as a CSTR. Finally, the logical arrangement of the subreactors will be several stages of a parallel PFR and CSTR transferring energy and mass at their exit. This concept is shown in Figure 3. In this figure, at each step, a feed stream enters a parallel CSTR and PFR, and heat and mass transfer are taken into account at the exit of each step.

To develop the governing equations on the proposed system of subreactor arrangement, the following assumptions were made:

(a) Reactions are taking place in both bubble and emulsion phases.[28]
(b) Generalized steady-state mass balance correlations are used to obtain bubble and emulsion phase hydrodynamic behaviors at each simulation stage.
(c) The temperature is not fixed inside the FBC, and its axial variation should be considered in the model.
(d) Bubbles are highly affected by the temperature variation; therefore, axial bubble size alteration should be taken into account in the model.
(e) The bed is not in the dense state (it is always fluidized).
(f) The emulsion may not stay at minimum fluidization state necessarily; however, it can contain extra gas at high gas velocities. Such a dynamic phase distribution is well addressed by dynamic two-phase model.[29,30]
(g) Elutriation of crushed solid is negligible (constant solid loading inside the bed).
(h) Average particle size is constant inside the bed; that is, no agglomeration in the bed materials is happening, and the volatile combustion takes place several orders of magnitude faster[31] than char burn-out.

2.1. Kinetic Submodel. Based on the discussion in the Introduction, the volatiles from coal can be suitably simulated by propane. The main focus of present study is on the volatile behavior. According to the numerous experimental works in the literature, it is sufficient to model a coal-free propane system to understand coal volatile behavior. Basically, in the experimental studies on coal combustion, coal is not used directly.[3,6,17] What is being done is to use sand plus char (as a product of coal combustion) along with propane simultaneously. Propane is accepted to be an excellent model material of volatiles obtained from coal combustion. Therefore, simulation of such a volatile matter is important in the gasification process simulation. Although complex mechanistic reaction pathways can be considered to describe the combustion, four main reactions are reported to be sufficient to take care of the kinetics inside the bed[20,32,33] of sand particles (i.e., reduction reactions can be eliminated):

$$C_3H_8 \rightarrow \frac{3}{2}C_2H_4 + H_2 \quad (1)$$

$$C_2H_4 + O_2 \rightarrow 2CO + 2H_2 \quad (2)$$

$$CO + \frac{1}{2}O_2 \rightarrow CO_2 \quad (3)$$

$$H_2 + \frac{1}{2}O_2 \rightarrow H_2O \quad (4)$$

Accordingly, four reaction rates are required[20,32,33] to have a properly defined reaction kinetic model. Equations 5−8 are the rates of reactions 1−4, respectively, per unit gas volume (m^3) per second:

$$d[C_3H_8]/dt = (2.57 \times 10^{13})[C_3H_8]^{0.5}[O_2]^{1.07}[C_2H_4]^{0.4} \exp[(-24962 \pm 1207)/T_G] \quad (5)$$

dx.doi.org/10.1021/ef300710j | Energy Fuels 2012, 26, 5199−5209

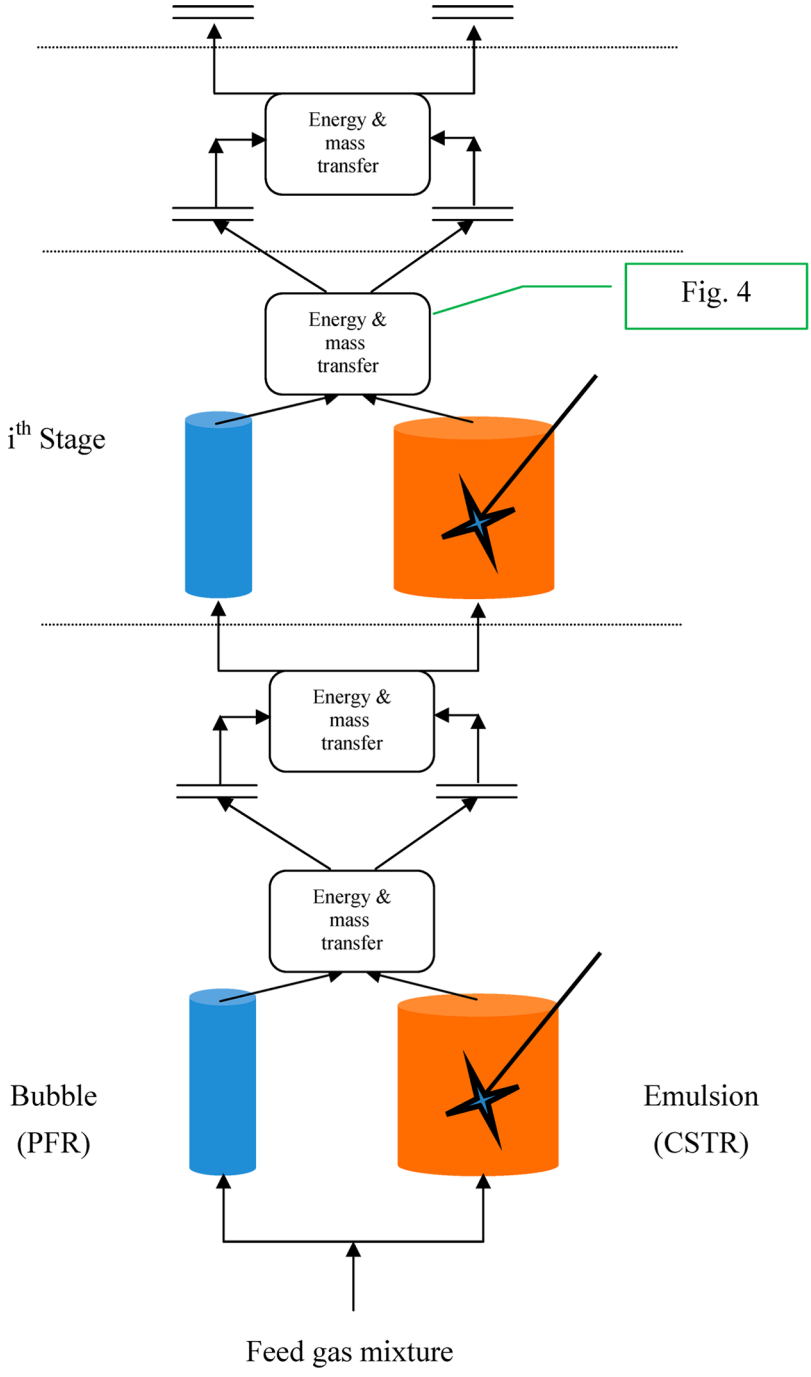

Figure 3. Schematic diagram of the sequential modular simulation of a dense bed.

$$d[C_2H_4]/dt = (3.71 \times 10^{12})[C_2H_4]^{0.9}[O_2]^{1.18}[C_3H_8]^{-0.37} \exp[(-25163 \pm 2516)/T_G] \quad (6)$$

$$d[CO]/dt = (2.23 \times 10^{12})[CO][O_2]^{0.25}[H_2O]^{0.5} \exp[(-20130 \pm 604)/T_G]S \quad (7)$$

$$d[H_2]/dt = (2.45 \times 10^{11})[H_2]^{0.85}[O_2]^{1.42}[C_2H_4]^{0.56} \exp[(-20634 \pm 3221)/T_G] \quad (8)$$

In the reaction rate of CO (eq 7), S is defined as

$$S = 7.93\, e^{-2.48\Phi} \quad (9)$$

in which Φ is the initial equivalence ratio.[20]

2.2. Hydrodynamic Submodel. Based on the reaction kinetic submodel, occurring reactions are highly exothermic; therefore, the bubble size is changing through the bed. The bubble growth phenomenon is simultaneous with the heat set free from the reaction. Considering an ideal gas behavior, the effect of temperature on bubble diameter variation is suggested[34] to be obtained using eq 10.

$$r_c = \left(\frac{T_b}{T_\infty}\right)^{1/3} r_{c,\infty} \quad (10)$$

Based on this equation, normalized cubic bubbles size is proportional to normalized bed temperature. At every stage of

dx.doi.org/10.1021/ef300710j | Energy Fuels 2012, 26, 5199–5209

the model, gas temperature inside the emulsion phase is considered to be constant due to rigorous mixing. Accordingly, the volume of emulsion phase can be contemplated constant because of the unchanged gas density inside it. However, the gas density is changing inside the bubbles, and the bubble phase is assumed to have a variant volume.[34] The molar balance in the emulsion and bubble phases is presented in eqs 11 and 12, respectively.

$$C_{\mathrm{Ae}(i-1)}U_{\mathrm{e}}A_{\mathrm{e}} - r_{\mathrm{A}(i)}V_{\mathrm{CSTR}(i)} + K_{\mathrm{be}}(C_{\mathrm{Ab}(i)} - C_{\mathrm{Ae}(i)}) V_{\mathrm{e}(i)}\left(\frac{\delta}{1-\delta}\right) - C_{\mathrm{Ae}(i)}U_{\mathrm{e}}A_{\mathrm{e}} = 0 \quad (11)$$

$$C_{\mathrm{Ab}(i-1)}U_{\mathrm{b}}A_{\mathrm{b}} - A_{\mathrm{b}}\varepsilon_{\mathrm{b}}\int_{z_{i-1}}^{z_i} r_{\mathrm{A}(i)}\,\mathrm{d}z - K_{\mathrm{be}}(C_{\mathrm{Ab}(i)} - C_{\mathrm{Ae}(i)}) V_{\mathrm{b}(i)} - C_{\mathrm{Ab}(i)}U_{\mathrm{b}}A_{\mathrm{b}} = 0 \quad (12)$$

The first and last term in eqs 11 and 12 account for bulk flow in and out, respectively, the second term is taking care of consumption or production of each species, and the third term considers the mass transfer. The mass transfer among the phases is calculated based on Figure 4. As illustrated in this figure, convection-based transfers inside each phase of bubble or emulsion, as well as conduction between these two phases, are playing a main role in transferring heat and mass. Also, the energy balance over the bubble phase can be described as eq 13.

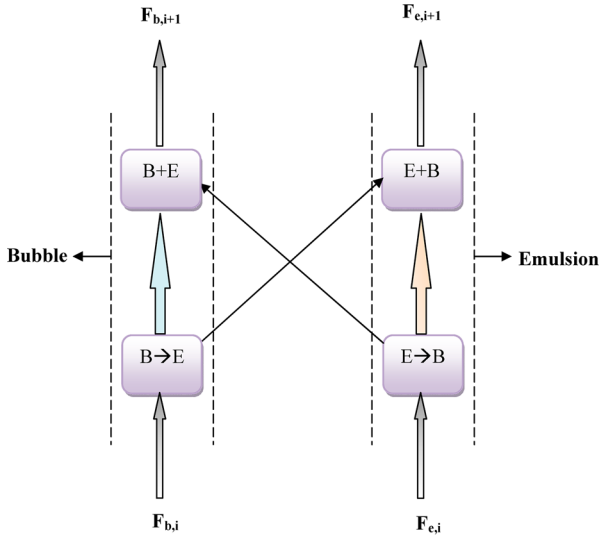

Figure 4. Schematic diagram of mass and energy transfer in a dense bed.

$$\sum_{j=1}^{n} C_{\mathrm{jb},(i)}C_{\mathrm{P}j,(i)}U_{\mathrm{b}}A_{\mathrm{b}}T_{\mathrm{b},(i)} - \sum_{j=1}^{n} C_{\mathrm{jb},(i-1)}C_{\mathrm{P}j,(i-1)}U_{\mathrm{b}}A_{\mathrm{b}}T_{\mathrm{b},(i-1)} - \Delta H A_{\mathrm{b}}\varepsilon_{\mathrm{b}}\int_{z_{i-1}}^{z_i} r_{\mathrm{A}(i)}\,\mathrm{d}z - 4\pi h_{\mathrm{be}}(T_{\mathrm{b},(i)} - T_{\mathrm{b},(i-1)}){r_{\mathrm{c}}}^2 = 0 \quad (13)$$

In this equation, the first two terms account for the net bulk flow in and/or out, the third term is considering the heat generation by the reactions occurring inside the reactor, and the last term is related to heat transfer from bubbles to the emulsion phase. The parameters needed to define the hydrodynamic submodel are listed in Table 1.[23,29,30,34−38]

After finishing the mass transfer calculations at each stage, i, the flow is properly distributed among the phases according to the dynamic two-phase model,[29,30] and the simulation gets into the next step, $i + 1$. The calculation at various bed heights continuous until the top of the bed is reached. The energy balance and bubble growth are also taken into account at the exit of each section simultaneously.

3. RESULTS AND DISCUSSION

After arranging the subreactors based on the nature of phases, first, two sets of experimental data were considered and simulated considering various numbers of simulation sections. The aim is to find the effect of simulation section number on the prediction ability of proposed model. CO_2 yield from Hesketh and Davidson's[6] experimental work was chosen and simulated using 1−5 simulation section(s) shown in Figure 5. The CO_2 yield (%) against reactor temperature is presented in Figure 5. As illustrated in this figure, all of the simulations at low temperature (1023 K) accurately predict the experimental yield. This is because the reaction kinetic, and accordingly the reactor temperature, is dominant over the hydrodynamics. At this condition, the yield is basically low and the reaction kinetic is the limiting step in defining the product. However, by an increase in temperature, the deviation in model predictions from experimental values is obvious. At a temperature of 1073 K, having 4 sections of subreactor sets leads to the best model prediction, as is obvious in Figure 5. At higher temperatures, (e.g., 1173 and 1223 K) 3 and 2 sections result in the best predictions, respectively. Such a nonpredictable trend of simulation results is the outcome of simultaneous effect of hydrodynamics and reaction kinetics, which are nonlinearly coupled together.

The second test on the simulation section-number effect on model prediction is conducted using the Ross et al. experiments.[3] The effect of reactor temperature on propane conversion is simulated based on the previously proposed model, and the results are shown in Figure 6. This figure depicts how an increase in bed temperature is increasing the propane conversion. As it is seen in Figure 6, at a temperature of 1023 K, 2 and 3 simulation sections are the best predictors, while at 1123 K, 3 stages result in the most accurate prediction. At a higher temperature, 1223 K, $n = 3$ shows the best prediction ability.

Figures 5 and 6 showed that the proposed sequential approach is able to predict real-life reactors successfully, but the main challenge is to define the number of simulation sections accurately to have the most precise predictions. The required number of simulation steps, as the most important part of a sequential-based modeling, is a function of several affecting physical and chemical parameters such as fluid (feed) superficial velocity, solid particle size, bed operating temperature, gas−solid relative density, actual air fed into the reactor, stoichiometric air, and reactants concentration. To find the effect of these parameters on the stage number, various sets of experimental data were considered.[3,6,17,39] Based on the comprehensive investigation on the experimental volatile combustion processes, three main branches of affecting phenomena, namely, hydrodynamics, reaction kinetics, and heat transfer, were found to be playing vital roles in such reactors.

dx.doi.org/10.1021/ef300710j | Energy Fuels 2012, 26, 5199−5209

Table 1. Required Hydrodynamic Parameters

param.	correlation	ref
Archimedes number	$\mathrm{Ar} = \frac{\rho_g d_p^{\,3}(\rho_p - \rho_g)g}{\mu_g^{\,2}}$	35
bubble diam.	$D_b = 0.21 H_f^{\,0.8}(U_0 - U_{mf})^{0.42} \exp[-0.25(U_0 - U_{mf})^2 - 0.1(U_0 - U_{mf})]$	36
min. fluidization velocity	$\frac{U_{mf}\rho_g d_p}{\mu_g} = \sqrt{27.2^2 + 0.0408\mathrm{Ar}} - 27.2$	37
bubble rise velocity	$U_{br} = 0.711\sqrt{gD_b}$	
bubble velocity	$U_b = U_0 - U_e + U_{br}$	23
emulsion velocity	$U_e = \frac{U_0 - \delta U_b}{1 - \delta}$	
bubble-to-emulsion mass transfer coefficient	$\frac{1}{K_{be}} = \frac{1}{K_{bc}} + \frac{1}{K_{ce}}$	38
	$\frac{1}{K_{bc}} = 4.5\left(\frac{U_e}{D_b}\right) + 5.85\left(\frac{D_{AB}^{\,1/2} g^{1/4}}{D_b^{\,5/4}}\right)$	
	$\frac{1}{K_{ce}} = 6.77\left(\frac{D_{AB}\epsilon_e U_{br}}{D_b^{\,3}}\right)^{1/2}$	
gas-to-particle heat transfer coefficient	$h_{gp,br} = \left(\frac{k_g}{d_p}\right)(2 + 0.6\mathrm{Re}_p^{\,1/2}\mathrm{Pr}_p^{\,1/3})$	34
bubble-to-emulsion heat transfer coefficient	$h_{be} = 0.25 U_{br} C_{p,p}\rho_p \epsilon_b \left\{1 - \exp\left[-6\tau\left(\frac{h_{gp,br}k_g}{k_s C_{p,p}\rho_p d_p}\right)\right]\right\}$	
voidage in bubble phase	$\epsilon_b = A_{\text{void-b(1)}} + A_{\text{void-b(2)}} \exp\left(-\frac{U_0 - U_{mf}}{A_{\text{void-b(3)}}}\right)$	
voidage in emulsion phase	$\epsilon_e = A_{\text{void-e(1)}} + A_{\text{void-e(2)}} \exp\left(-\frac{U_0 - U_{mf}}{A_{\text{void-e(3)}}}\right)$	29 and 30
emulsion fraction	$\delta = 1 - A_{f(1)} - A_{f(2)} \exp\left(-\frac{U_0 - U_{mf}}{A_{f(3)}}\right)$	
residence time of particle in bubble	$\tau = \sqrt{2.3 r_c/g}$	34

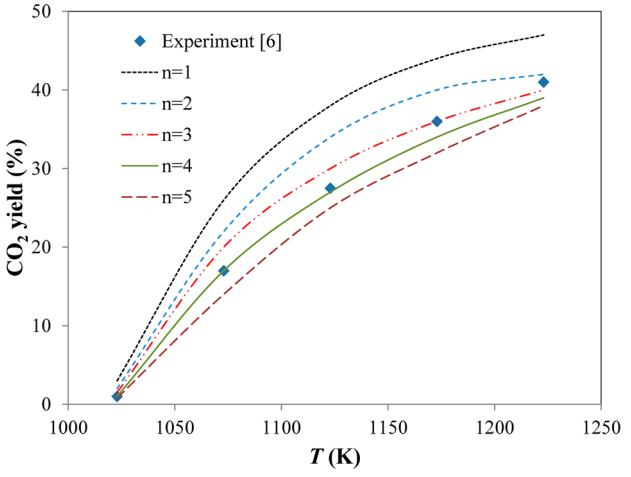

Figure 5. CO_2 yield as a function of bed temperature at different number of sections: comparison between the model and experiments,[6] the values of Q_S for the experimental data (T = 1023−1223 K) are 15.3, 16.1, 17.9, 22.6, and 27.1, respectively.

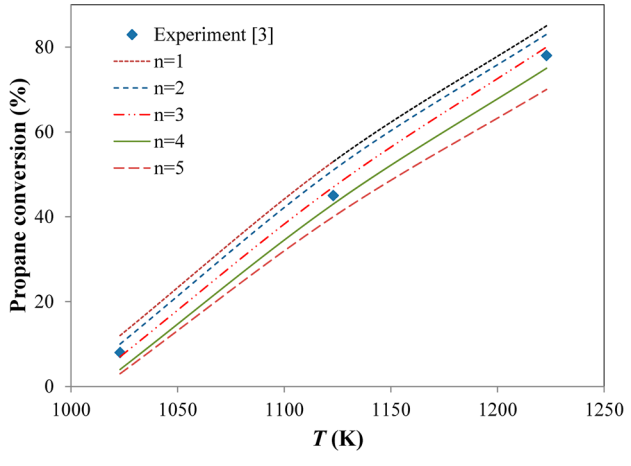

Figure 6. Propane conversion as a function of bed temperature at different number of sections. Comparison between the model and experiments,[3] the values of Q_S for the experimental data (T = 1023−1223 K) are 18.7, 23.3, and 25.9, respectively.

From the hydrodynamic point of view, three main parameters were found to be effective: gas−solid relative

dx.doi.org/10.1021/ef300710j | Energy Fuels 2012, 26, 5199−5209

Table 2. Experimental Operating Conditions

param.	unit	3	6	17	39
H	m	0.16	0.18	0.3	0.24
D	m	0.01	0.069	0.08	0.076
d_p	μm	350−500	410	250−500	327
ρ_s	kg/m^3	2643	2650	2650	2650
T_{bed}	°C	750−950	750−950	400−900	750−850
T_0	°C	25	500	25	47
P	Pa	101300	101300	101300	101300
α		2	2.5	1.62−1.98	1.6
U	mm/s	63	58	47−58	43

density, the ratio of gas velocity to minimum fluidization velocity, and bed aspect ratio (bed height over bed diameter). Also, bed critical temperature (defined as the temperate below which no reaction occurs inside the bed[11,34]), bubble-to-emulsion heat transfer coefficient, and gas and solids specific heat capacities are found as the main kinetics and heat transfer-related operating parameters, respectively. It is noteworthy that the bed temperature has also a crucial effect on the combustion reaction kinetics.

Starting from hydrodynamic parameters, the higher the gas−solid relative density (i.e., the higher the Archimedes number), the more difficult it is to fluidize the particles and have the bed ready for volatile combustion. In contrast, by the increase of superficial feed gas velocity, the bed approaches its fluidized state and gets ready for having a complete combustion reaction. Also, an increase in gas velocity leads to enhanced heat transfer between solid and gas phase due to better mixing at fluidized condition compared to a fixed-solid bed. Furthermore, bubble-phase volume fraction in the bed is dependent on bed aspect ratio. Increasing bed aspect ratio increases bubble residence time inside the bed and, consequently, gives rise to a higher bubble volume fraction. Basically, an increase of bubble volume fraction provides more volume for combustion reaction because the main phase in which the combustion reaction takes place is gas bubbles.[20] Accordingly, for example, an increase in aspect ratio, which increases bubble volume fraction, leads to higher conversion; therefore, to predict accurate conversions, simulation stages should be decreased (i.e., conversion is nonlinearly and inversely proportional to aspect ratio).

Besides, the location of combustion reactions is a vital characteristic of such reactors. van der Vaart[39] demonstrated that the ignition front moves closer to distributor by the increase of particle size and bed temperature as well as the decrease of excess gas velocity. In addition, Dennis et al.[9] showed that a critical temperature exists in combustion processes, which varies according to the type of fluidized beds. Below the so-called critical temperature, the combustion may shift toward the freeboard region. It is shown that, above the combustion critical temperature, the emulsion phase exhibits homogeneous combustion behavior in a fluidized bed reactor.[40,41]

Also, an increase in solid loading in a reactor, which increases static bed height, leads to a decrease in bed temperature because higher bed heights result in higher gas residence time inside the bed, which finally gives rise to gentle combustion of feed with less gas bursting in the freeboard section. Ribeiro and Pinho[42] showed that the critical temperature increases as the sand size increases. The main reason for this is the enhanced through-bubble advective flow rate, which gives rise to more severe removal of species generated by the reactions inside the bubbles, that is, C_2H_4, from within the bubbles.

The surface-to-volume effect limits the in-bed ignition;[39] therefore, the increase of excess fluidizing velocity $(U - U_{mf})$ decreases critical temperature as a result of decreased gas interchange between bubble and emulsion phases. On the other hand, the bubble residence time decreases by increasing excess fluidization velocity.[39] Thus, the in-bed conversion will be decreased, which leads to shifting the ignition well above the bed surface. Consequently, at a high excess fluidizing velocity (Re/Re_m greater than or equal to 3), it was found that residence time has the main contribution in the in-bed combustion, which results in the increase of critical temperature by increasing superficial gas velocity. However, at fluidizing velocities near the minimum fluidization condition ($Re/Re_m < 3$), low surface area of the bubbles is the dominant phenomena, which results in lower critical temperatures. To obtain the critical temperature of coal's volatile combustion in fluidized bed reactors, various sets of experimental data were analyzed. Accordingly, based on several sensitivity tests on the reported experiments,[9,39,43] the effect of operating condition on the critical temperature was correlated and presented as eq 14:

$$T_{cr} - T_0 = C \ln\left(\frac{d_P\left(\frac{U - U_{mf}}{U_{mf}}\right)^n}{L_s}\right) \quad \begin{cases} \frac{Re}{Re_m} \geq 3 & n = 0.5 \\ \frac{Re}{Re_m} < 3 & n = -0.5 \end{cases} \tag{14}$$

In eq 14, T_0 and C are constants, which are found to be 1268, and 32.54 K, respectively, and L_s is the static bed height of solids loaded in the bed. T_0 is obtained from a least-squared curve fitting, which is in a good agreement with the maximum bed temperature reported in the experimental combustion literature.

The most important part of a sequential modular model, after logically arranging the subreactors, is to find the optimum number of stages to obtain the most accurate predictions. Four series of experiments were employed to cover a wide range of operating conditions to propose a method for obtaining optimum number of simulation stages. Properties and operating conditions of each case are presented in Table 2.[3,6,17,39] Based on the previous discussion on the influencing hydrodynamic, heat transfer, and reaction parameters, the following dimensionless number (Q_S) is proposed according to thorough sensitivity analyses to predict the generalized number of simulation steps in coal volatile combustion processes. This should be used along with the sequential approach for fluidized bed volatile combustion reactors behavior forecasting:

dx.doi.org/10.1021/ef300710j | Energy Fuels 2012, 26, 5199−5209

$$Q_S = 3.356 \times 10^3 \left[\left(\frac{Re_m}{Re}\right)^5 \left(\frac{(\rho_s - \rho_g) C_{pg} U_0}{h_{be}}\right)\right]^{0.4} \left[\frac{1}{\alpha}\right]^{(0.3T_{bed}/T_{cr})} \left[\exp\left(\frac{16186 - 12.8T_{bed}}{T_{bed}}\right)\right] [AR]^{-3} \quad (15)$$

in which Re_m is the particle Reynolds number at minimum fluidization velocity, h_{be} is bubble-to-emulsion heat transfer coefficient, and α is the air factor defined as the ratio of actual air volume fed into a FBC to stoichiometric air volume . The relationship between the number of stages and the dimensionless number, Q_S, in various operating conditions of fluidized bed combustors is presented in Table 3. In each case, all the

Table 3. Number of Stages (n) Defined by Q_S Dimensionless Number

Q_S	n
$Q_S \geq 37.8$	1
$26.5 \leq Q_S < 37.8$	2
$18.2 \leq Q_S < 26.5$	3
$10.3 \leq Q_S < 18.2$	4
$Q_S < 10.3$	5

affecting parameters, except one, for example, bed temperature, are considered to be constant, and then, the desired parameter was manipulated to calculate the proper effect on the proposed dimensionless number.

Employing the optimum number of simulation stages, the propane conversion profile along the combustor height is calculated using the so-called sequential model, which is shown in Figure 7. As illustrated in Figure 7, propane conversion

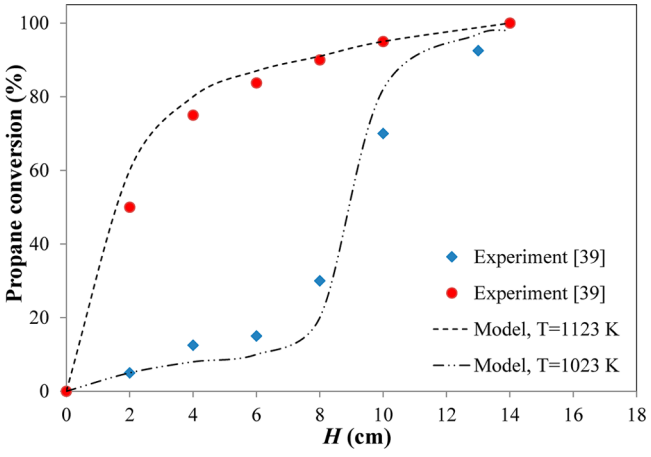

Figure 7. Propane conversion along the fluidized bed combustor at two different bed temperatures, obtained using the optimum number of simulation stages at each operating condition.

increases by the increase in reactor height. However, different operating temperatures result in different conversion behavior. Operation at a temperature of 1023 K leads the reaction toward the combustor freeboard; therefore, propane conversions higher than 20% start at heights larger than 8 cm from the reactor distributor. However, at a temperature of 1123 K, the combustion starts right above the distributor and the conversion reaches more than 80% at a bed height equal to 6 cm. It is clear that simulation results are predicting the experimental conversions accurately.

So far, the variation of bubble diameter, as a crucial parameter in the hydrodynamics of fluidized bed combustors, has been taken into consideration parallel to the sequential model. It can be of industrial interests to have an estimation of neglecting the bubble diameter alteration on the model predictions. Such an important effect is demonstrated in Figure 8, which presents propane conversion along the fluidized bed

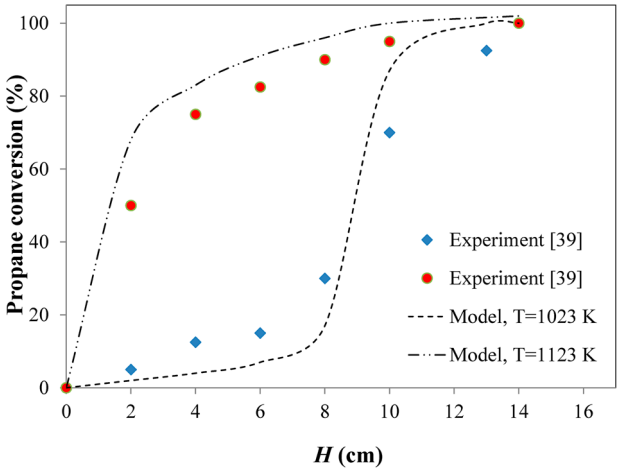

Figure 8. Propane conversion along the fluidized bed at two different temperatures, without considering bubble growth.

reactor at two different temperatures, considering bubbles to have a constant size. Moreover, the model results are compared to the experimental data at two bed temperatures, and error statistics are shown in Table 4. Variation of bubble diameter is depending on the bubble temperature. These two physical characteristics of volatile combustion reactors are interrelated by eq 10. Accordingly, the assumption of having constant bubble size results in higher relative errors. This, especially, occurs at high temperatures, which has been confirmed in Table 4.

To test the accuracy of proposed simulation method, predicted propane conversions versus the experimental conversions reported in the literature[3,39] are gathered in a parity plot, which is presented in Figure 9. This figure shows the propane conversion percentage based on the model against those reported in the literature. It can be seen in Figure 9 that the suggested simulation method is applicable in the whole range of propane conversions from 0−100%. Model predictions without considering bubble size variations are also illustrated in Figure 9. Furthermore, to quantify the prediction accuracy of current method, the model performance was evaluated quantitatively using error statistics, that is, BIAS and scatter index (SI), defined as follows:

$$BIAS = \sum_{i=1}^{N} \frac{1}{N}(Y_i - X_i) \quad (16)$$

and

$$SI = \frac{\sqrt{\frac{1}{N}\sum_{i=1}^{N}(Y_i - X_i)^2}}{\bar{X}_i} \quad (17)$$

dx.doi.org/10.1021/ef300710j | Energy Fuels 2012, 26, 5199−5209

Table 4. BIAS, Scatter Index (SI), and Correlation Coefficient (CC) of Model Results for Bubble Diameter Variations

	BIAS		SI		CC	
bubble diameter	T = 1023 K	T = 1123 K	T = 1023 K	T = 1123 K	T = 1023 K	T = 1123 K
constant: 0.024 m	−0.19	0.25	0.15	0.18	0.98	0.97
growing bubbles	−0.11	0.16	0.12	0.09	0.96	0.98

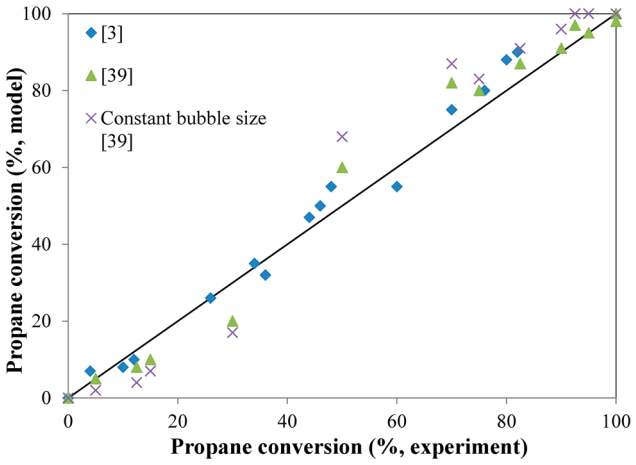

Figure 9. Comparison between the experimental data and the model predictions in term of propane conversion.

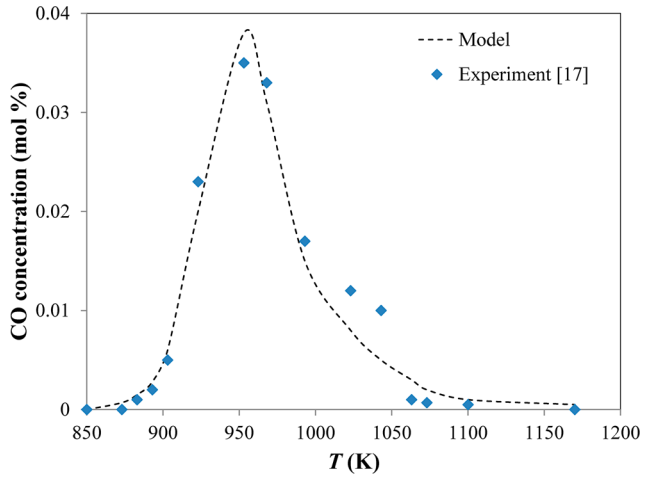

Figure 10. CO concentration versus bed temperature: comparison between the model and experiments,[17] CC = 0.95.

where X_i and Y_i represent the experimental and predicted values, respectively, and N is the total observations number. $\bar{X}$ is the experimental data mean value. Moreover, correlation coefficient (CC) is calculated for each set of experiments based on eq 18:

$$\mathrm{CC} = \frac{\sum_{i=1}^{N}(X_i - \bar{X})(Y_i - \bar{Y})}{\sqrt{\sum_{i=1}^{N}(X_i - \bar{X})^2 \sum_{i=1}^{N}(Y_i - \bar{Y})^2}} \quad (18)$$

In eq 18, $\bar{Y}$ is the mean value of predicted data. Measured errors, presented in Table 5, are remarkably low, so that they confirm the validity of the proposed model.

Table 5. BIAS, Scatter Index (SI), and Correlation Coefficient (CC) of Model Results for Various Number of Sections

reactor result	BIAS	SI	CC
3	−0.11	0.07	0.99
6	−0.07	0.10	0.98
17	−0.09	0.12	0.95
39	0.09	0.06	0.96

It is important to examine the applicability of the model in determining effluent gases production amount. This is of a high importance in coal gasification processes, especially from the environmental point of view. To pursue this purpose, effluent CO concentration as a function of bed temperature is obtained and presented in Figure 10. It can be observed in this figure that increasing bed temperature gives rise to an increased CO concentration until a certain temperature is reached. This is the so-called critical temperature. At temperatures lower than the critical temperature, as discussed earlier, bubbles explode in the freeboard, and consequently, sand particles cool the incoming gases in the bed and act as combustion inhibitors. Such phenomenon leads to an incomplete volatile combustion inside the bed, which results in the increased CO concentration. In contrast, at high enough temperatures, the reaction zone shifts toward the distributor and bubbles explode at early stages inside the bed, which ensures a sufficient time for a complete combustion and conversion of CO into CO_2. To capture CO concentration evolution at different bed heights, two temperatures were chosen to study the conditions of both lower and higher temperatures than the critical temperature. Figure 11

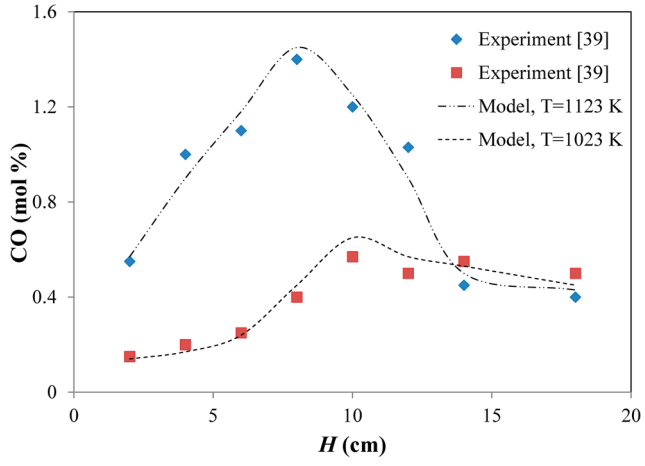

Figure 11. CO concentration versus bed height: comparison between the model and experiments,[39] CC = 0.93 and 0.91 for T = 1023 and 1123 K, respectively.

shows the CO concentration versus bed height at two temperatures of 1023 K (lower than T_{cr}) and 1123 K (higher than T_{cr}). As can be seen in this figure, at a temperature higher than the critical temperature, a maximum in CO concentration is achieved at the middle of the reactor. This is attributed to the gradual combustion of feed gas inside the bed, which leads to prevailing CO production up to the middle of bed and then

dx.doi.org/10.1021/ef300710j | Energy Fuels 2012, 26, 5199−5209

prevailing CO_2 production over CO up to the reactor exit. However, at a temperature (T = 1023 K) lower than the critical temperature, it is concluded from Figure 11 that no obvious maximum value in CO concentration is achieved. In fact, at low temperatures, reported explosive combustion[39] in the freeboard is causing an incomplete CO conversion to CO_2, which then results in a plateau in the CO concentration at higher bed heights. Based on Figure 11, the model proves to be successful in capturing experimental CO concentrations.

Ethylene production yield, defined as the produced species over the inlet propane, is also calculated and shown in Figure 12. This figure presents the yield of an important intermediate

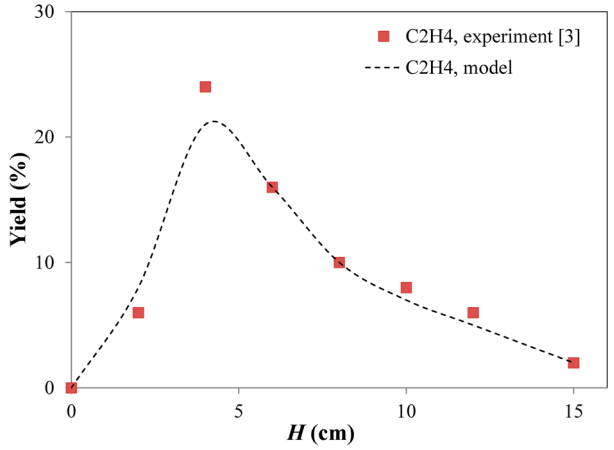

Figure 12. C_2H_4 yield along the fluidized bed reactor: comparison between the model and experiments,[3] CC = 0.93.

species, namely ethylene, at various bed heights. The yield profile is illustrated along the fluidized bed reactor at a bed temperature of 1223 K. As can be seen in Figure 12, C_2H_4 yield rises continuously up to approximately one-third of the bed height and decreases rapidly at a location where a high temperature occurs. The increase of temperature confronts the inhibition effects of solid particles in the bed, which leads to a continuous conversion of species.

Effluent CO_2 is also been focused in this study. The effect of bed temperature on CO_2 production volume percent was obtained using the sequential modular model and presented along with the experimental data in Figure 13. Increase in reactor temperature increases the CO_2 production monotonically, as can be seen in Figure 13. However, effluent CO_2 volume percent increases slowly at high temperatures (approximately, $T > T_{cr}$) compared to relatively lower temperatures (approximately, $T < T_{cr}$). This is due to approaching maximum in-bed kinetic conversion based on the simultaneous reactions presented in eqs 5−8. Again, the model proves to be successful in predicting the effluent gases production amounts in the experimental reactors.

4. CONCLUSION

A sequential method for coal volatile combustion, simulated by propane, was employed to predict the behavior of corresponding fluidized bed reactors in coal gasification processes. A fluidized bed reactor was divided into several subreactors based on a fundamental analysis of main physical and chemical events occurring inside it. The subreactors were connected in an intelligent manner to mimic real industrial reactors. The behavior of each subreactor was expressed according to well-

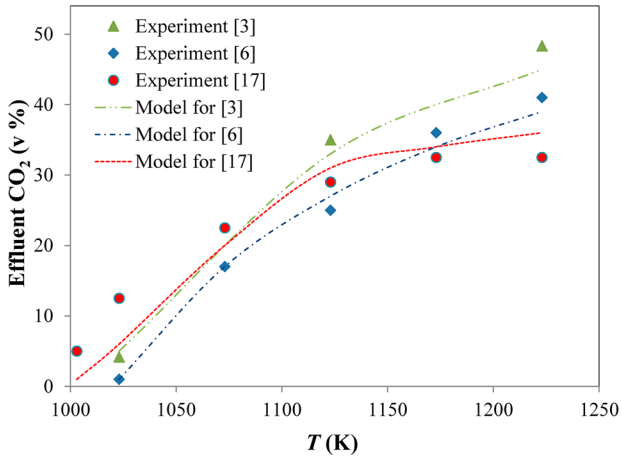

Figure 13. CO_2 production as a functions of bed temperature, CC = 0.98, 0.98, and 0.96 for refs 3, 6, and 17, respectively.

known unit operations in chemical engineering. Heat and mass transfer were considered simultaneously at each simulation stage, and the dynamic two-phase model was used for the hydrodynamic characterization of interacting phases inside the multiphase reactor. Furthermore, a new dimensionless number was introduced to specify accurate required simulation stages. It was shown that the proposed method can successfully predict coal's volatile matter combustion behavior without any further need for solving coupled nonlinear differential equations in an equation-oriented manner. Ease of conduct, ability to integrate with industrial process simulation packages, accuracy of predictions, and fundamental chemical engineering concepts usage are the main characteristics of the model.

AUTHOR INFORMATION

Corresponding Author

*Fax: +98 21 6646-1024. Email: sotudeh@ut.ac.ir.

Present Address

‡Chemical Engineering Department, McGill University, Montreal, Quebec H3A 2B2, Canada

Author Contributions

†These authors contributed equally to this work

Notes

The authors declare no competing financial interest.

NOMENCLATURE

A = cross-sectional area (m^2)
$A_{f(1)}$ = constant of the dynamic two-phase model
$A_{f(2)}$ = constant of the dynamic two-phase model
$A_{f(3)}$ = constant of the dynamic two-phase model
$A_{void\text{-}b(1)}$ = constant of the dynamic two-phase model
$A_{void\text{-}b(2)}$ = constant of the dynamic two-phase model
$A_{void\text{-}b(3)}$ = constant of the dynamic two-phase model
$A_{void\text{-}e(1)}$ = constant of the dynamic two-phase model
$A_{void\text{-}e(2)}$ = constant of the dynamic two-phase model
$A_{void\text{-}e(3)}$ = constant of the dynamic two-phase model
Ar = Archimedes number, $((d_p{}^3\rho_g(\rho_p - \rho_g)g)/\mu_g{}^2)$
AR = aspect ratio
BIAS = bias of data
C_A = concentration of component A (mol/m^3)
C_p = molar specific heat capacity (J/(mol·K))
$C_{p,m}$ = specific heat capacity (J/(kg·K))
CC = correlation coefficient

dx.doi.org/10.1021/ef300710j | Energy Fuels 2012, 26, 5199−5209

d_p = particle diameter (m)
D = bed diameter (m)
D_{AB} = diffusion coefficient (m^2/s)
D_b = bubble mean diameter (m)
D_r = reactor diameter (m)
f = emulsion phase fraction
$F_{b,in}$ = flow entering the bubble phase (mol/s)
$F_{b,out}$ = flow exiting the bubble phase (mol/s)
$F_{e,in}$ = flow entering the emulsion phase (mol/s)
$F_{e,out}$ = flow exiting the bubble phase (mol/s)
g = acceleration of gravity (m/s^2)
H = reactor height (m)
ΔH = heat of combustion of methane (J/mol)
h_{be} = bubble-emulsion heat-transfer coefficient ($W/(m^2 \cdot K)$)
$h_{gp,br}$ = gas-to-particle heat transfer coefficient based on U_{br} ($W/(m^2 \cdot K)$)
H_f = bubbling bed height (m)
k = thermal conductivity ($W/(m \cdot K)$)
K_{bc} = bubble-to-cloud mass transfer coefficient (1/s)
K_{be} = bubble-to-emulsion mass transfer coefficient (1/s)
K_{ce} = cloud-to-emulsion mass transfer coefficient (1/s)
L_s = static bed height (m)
n = number of stages
N = number of observations
N_S = proposed combustion dimensionless number
Pr = Prandtl number, $(C_p\mu/k)$
Q_S = proposed dimensionless number to obtain optimum simulation stages
R = universal gas constant ($kJ \cdot mol^{-1} \cdot K^{-1}$)
Re = Reynolds number
Re_m = Reynolds number at minimum fluidization condition
r_A = reaction rate with respect to component A ($mol/(m^3 \cdot s)$)
r_c = bubble radius (m)
$r_{c,\infty}$ = bubble radius at T_∞ in the absence of reaction (m)
T = temperature (K)
T_∞ = bed temperature (K)
T_b = favored temperature to calculate bubble radius at (K)
t = time (s)
U_b = bubble velocity (m/s)
U_{br} = bubble rise velocity (m/s)
U_e = emulsion gas velocity (m/s)
U_{mf} = minimum fluidization velocity (m/s)
U_0 = superficial gas velocity (m/s)
V_b = bubble-phase volume (m^3)
V_{CSTR} = emulsion-phase volume (m^3)
X_i = experimental values
$\overline{X}$ = mean value of experimental data
Y_i = predicted values
$\overline{Y}$ = mean value of predicted values
z = distance from distributor (m)

Greek Symbols

α = air factor
δ = bubble phase fraction
ε = average bed porosity
ε_b = bubble phase porosity
ε_e = emulsion phase porosity
Φ = initial equivalence ratio
μ_g = gas viscosity (Pa·s)
ρ_g = gas density (kg/m^3)
ρ_p = particle density (kg/m^3)
τ = residence time of particles inside the bubble phase (s)

Subscripts

b = bubble phase
c = in the absence of chemical reaction
e = emulsion phase
g = gas
mf = evaluated at minimum fluidizing velocity
p = particle

REFERENCES

(1) Hanne, G. A. The energy crisis in southern South America: The importance of coal deposits. *Neues Jahrbuch fur Geologie und Palaontologie—Abhandlungen* **2009**, *253* (1), 3−14.
(2) Goldmeer, J. Gasification offers a cleaner goal solution. *Power Eng.* **2011**, *115* (11), 28−34.
(3) Ross, D. P.; Yan, H. M.; Zhang, D. K. An experimental study of propane combustion in a fluidized-bed gasifier. *Combust. Flame* **2001**, *124* (1−2), 156−164.
(4) Borah, R. C.; Ghosh, P.; Rao, P. G. A review on devolatilization of coal in fluidized bed. *Int. J. Energy Res.* **2011**, *35* (11), 929−963.
(5) Stubington, J. F. Role of coal volatiles in fluidized bed combustion. *J. Inst. Energy* **1980**, *53* (417), 191−195.
(6) Hesketh, R. P.; Davidson, J. F. The effect of volatiles on the combustion of char in a fluidized bed. *Chem. Eng. Sci.* **1991**, *46* (12), 3101−3113.
(7) Stubington, J. F.; Chan, S. W. On the phase location and rate of volatiles combustion in bubbling fluidized bed combustors. *Chem. Eng. Res. Des.* **1990**, *68* (2), 195−201.
(8) van der Vaart, D. R. The chemistry of premixed hydrocarbon/air combustion in a fluidized bed. *Combust. Flame* **1988**, *71* (1), 35−39.
(9) Dennis, J. S.; Hayhurst, A. N.; Mackley, I. G. The ignition and combustion of propane/air mixtures in a fluidized bed. *Symp. (Int.) Combust.* **1982**, *19* (1), 1205−1212.
(10) Hayhurst, A. N. Does carbon monoxide burn inside a fluidized bed? A new model for the combustion of coal char particles in fluidized beds. *Combust. Flame* **1991**, *85* (1−2), 155−168.
(11) Hesketh, R. P.; Davidson, J. F. Combustion of methane and propane in an incipiently fluidized bed. *Combust. Flame* **1991**, *85* (3−4), 449−467.
(12) Sotudeh-Gharebagh, R.; Chaouki, J. The heterogeneous and homogeneous combustion of methane over inert particles. *Can. J. Chem. Eng.* **2003**, *81* (6), 1182−1191.
(13) Sotudeh-Gharebagh, R.; Chaouki, J. Development of a clean fluidized bed reactor for food-grade CO_2 production. *Int. Energy J.* **2003**, *4* (1), 41−52.
(14) Sotudeh-Gharebagh, R.; Chaouki, J.; Sauriol, P. An experimental study of non-premixed combustion in a turbulent fluidized-bed reactor. *Fuel Process. Technol.* **2007**, *88* (9), 847−858.
(15) Sotudeh-Gharebaagh, R.; Chaouki, J. Investigation of highly exothermic reactions in a turbulent fluidized bed reactor. *Energy Fuels* **2007**, *21* (4), 2230−2237.
(16) van der Vaart, D. R.; van der Vaart, H. R. Use of a second endothermic reaction to desensitize a tubular reactor. *AIChE J.* **1991**, *37* (2), 225−232.
(17) Ribeiro, L.; Pinho, C. Generic behaviour of propane combustion in fluidized beds. *Chem. Eng. Res. Des.* **2004**, *82* (12), 1597−1603.
(18) Ross, D. P.; Laurent, P. J.; Schluter, G. B.; Zhang, D. K. Influence of volatiles on combustion rate of Loy Yang coal char in a fluidized bed combustor. *Dev. Chem. Eng. Miner. Process.* **2000**, *8* (3), 187−198.
(19) Bautista-Margulis, R. G.; Chacon-Nava, J. G.; Arias Del Campo, E.; Almeraya-Calderon, F.; Gaona-Tiburcio, C.; Martínez-Villafañe, A. Modeling of volatiles combustion and alkali deposition in a fluidized bed coal combustor. *Chem. Eng. Technol.* **2002**, *25* (1), 83−90.
(20) Srinivasan, R. A.; Sriramulu, S.; Kulasekaran, S.; Agarwal, P. K. Mathematical modeling of fluidized bed combustion. 2: Combustion of gases. *Fuel* **1998**, *77* (9−10), 1033−1049.
(21) V. Flores, D.; H. Fletcher, T. A two mixture fraction approach for modeling turbulent combustion of coal volatiles and char oxidation

products. *Spring Meeting of the Central States/Western States/ Mexican National Sections of the Combustion Institute and the American Flame Research Committee* **1995**, *24*, 1767−1770.
(22) Yu, L.; Lu, J.; Zhang, X.; Zhang, S. Numerical simulation of the bubbling fluidized bed coal gasification by the kinetic theory of granular flow (KTGF). *Fuel* **2007**, *86* (5−6), 722−734.
(23) Kunii, D.; Levenspiel, O. *Fluidization Engineering*; Wiley: New York, 1969.
(24) Rhinehart, R. R.; Felder, R. M.; Ferrell, J. K. Coal gasification in a pilot-scale fluidized bed reactor. 3. Gasification of a Texas lignite. *Ind. Eng. Chem. Res.* **1987**, *26* (10), 2048−2057.
(25) Ross, D. P.; Yan, H.-m.; Zhang, D.-k. Modelling of a laboratory-scale bubbling fluidized-bed gasifier with feeds of both char and propane. *Fuel* **2004**, *83* (14−15), 1979−1990.
(26) Habibi, R.; Hajizadeh, S.; Sotudeh-Gharebagh, R.; Mostoufi, N. Two-phase sequential simulation of a fluidized bed reformer. *Chem. Eng. Technol.* **2008**, *31* (7), 984−989.
(27) Sarvar-Amini, A.; Sotudeh-Gharebagh, R.; Bashiri, H.; Mostoufi, N.; Haghtalab, A. Sequential simulation of a fluidized bed membrane reactor for the steam methane reforming using ASPEN PLUS. *Energy Fuels* **2007**, *21* (6), 3593−3598.
(28) Kiashemshaki, A.; Mostoufi, N.; Sotudeh-Gharebagh, R. Two-phase modeling of a gas phase polyethylene fluidized bed reactor. *Chem. Eng. Sci.* **2006**, *61* (12), 3997−4006.
(29) Cui, H.; Mostoufi, N.; Chaouki, J. Characterization of dynamic gas-solid distribution in fluidized beds. *Chem. Eng. J* **2000**, *79* (2), 133−143.
(30) Cui, H.; Mostoufi, N.; ChaoGbri, J. Gas and solids between dynamic bubble and emulsion in gas-fluidized beds. *Powder Technol.* **2001**, *120* (1−2), 12−20.
(31) Smith, I. W. The combustion rates of coal chars: A review. *Symp. (Int.) Combust.* **1982**, *19* (1), 1045−1065.
(32) Dryer, F. L.; Glassman, I. High temperature oxidation of CO and CH_4. In *Proceedings of the 14th Symposium (International) on Combustion*; The Combustion Institute: Pittsburgh, PA, 1973; pp 987−1003.
(33) Hautman, D. J.; Dryer, F. L.; Schug, K. P.; Glassman, I. Multiple-step overall kinetic mechanism for the oxidation of hydrocarbons. *Combust. Sci. Technol.* **1981**, *25* (5−6), 219−235.
(34) van der Vaart, D. R. Mathematical modeling of methane combustion in a fluidized bed. *Ind. Eng. Chem. Res.* **1992**, *31* (4), 999−1007.
(35) Wen, C. Y.; Yu, Y. H. A generalized method for predicting the minimum fluidization velocity. *AlChE J.* **1966**, *12* (3), 610−612.
(36) Cai, P.; Schiavetti, M.; De Michele, G.; Grazzini, G. C.; Miccio, M. Quantitative estimation of bubble size in PFBC. *Powder Technol.* **1994**, *80* (2), 99−109.
(37) Grace, J. R. Fluidized-bed hydrodynamics. In *Handbook of Multiphase Systems*, 5th ed.; Hestroni, G., Ed.; Hemisphere: Washington, DC, 1982; p 8.
(38) Davidson, J. F.; Harrison, D. *Fluidised Particles*; Cambridge University Press: Cambridge, U.K., 1963.
(39) van der Vaart, D. R. Freeboard ignition of premixed hydrocarbon gas in a fluidized bed. *Fuel* **1988**, *67* (7), 1003−1007.
(40) Hayhurst, A. N. Does carbon monoxide burn inside a fluidized bed? A new model for the combustion of coal char particles in fluidized beds. *Combust. Flame* **1991**, *85* (1−2), 155−168.
(41) Hayhurst, A. N.; Tucker, R. F. The combustion of carbon monoxide in a two-zone fluidized bed. *Combust. Flame* **1990**, *79* (2), 175−189.
(42) Ribeiro, L.; Pinho, C. A simple approach to numerical modeling of propane combustion in fluidized beds. *Chem. Eng. Commun.* **2009**, *196* (3), 305−329.
(43) Laviolette, J.-P.; Patience, G. S.; Chaouki, J. Non-premixed fluidized bed combustion of C1−C4 *n*-alkanes. *Fuel* **2011**, *90* (9), 2850−2857.